CAV2009 – Paper No. 107

A modified SST k-ω Turbulence Model to Predict the Steady and Unsteady Sheet Cavitation on 2D and 3D Hydrofoils

Da-Qing Li
SSPA Sweden AB
Göteborg, Sweden

Mikael Grekula
SSPA Sweden AB
Göteborg, Sweden

Per Lindell
SSPA Sweden AB
Göteborg, Sweden

ABSTRACT

The paper presents a study of using a modified SST (Shear-Stress Transport) k-ω model with a multi-phase mixture flow RANS solver to predict the steady and unsteady cavitating flows around 2D and 3D hydrofoils. Based on Reboud et al [6]'s idea of modifying turbulent viscosity for a RNG k-ε model, a modification is applied to a SST k-ω model in the present work. The cavitation is modeled by Schnerr-Sauer's cavitation model [16]. First, results of 2D NACA0015 foil at two cavitation numbers, σ=1.6 (stable sheet cavitation) and σ=1.0 (unsteady with shedding) are compared for different grids and with available experiment data. Then, the problem of the standard SST model in predicting unsteady cavitation is discussed. Finally the results for a 3D twisted hydrofoil are compared with the experiment by Foeth and Terwisga [3]. It is found that with the modified SST k-ω model the RANS solver is able to predict the essential features like development of re-entrant jets, the pinch-off, the shedding of vortex and cloud cavities for the 2D NACA0015 foil at σ=1.0. For the case at σ=1.6, the model predicts a high frequency fluctuating sheet cavity with minor shedding at its closure. Compared with the standard SST model, the global quantities like lift, drag, and shedding frequency predicted by the modified model are closer to the experimental data, although considerable discrepancy with the experiment data is noted for the unsteady case at σ=1.0. In addition, a special type of secondary cavities, developed downstream an upstream-moving collapse cavity and termed as "vortex group cavitation" by Bark et al [1], appears to be observable in the simulation at this condition. The existence of this type of cavity has been reconfirmed in a recent experiment in the SSPA's cavitation tunnel.

INTRODUCTION

The development of unsteady sheet cavitation on marine propellers calls for special concern, particularly when the sheet cavity is followed by a regular shedding of cloud structures, or the sheet cavity itself is performing a fast collapse. In addition to the adverse effects of noise, pressure pulsation and vibration caused by cavitation, the occurrence of a very fast and energy-focusing collapse of cavities is often related to risk of erosion [1][2]. Although experimental observations using the high-speed video recording techniques are indispensable tools for studying and solving cavitation problems today, advancement of computing power and numerical methods open up new possibilities to study the behavior of cavitation dynamics in detail. A short review of the experimental and computational work for the sheet cavitation was given by the authors in [13]. Our present approach is to use the single-fluid mixture flow RANS method based on the assumption of homogenous mixture of multi-phases.

Several recent work and our own numerical studies find that (a) the cavitating flow in the mixture-phase region is locally compressible [7][10][11][27]; (b) the standard two-equation turbulence models (e.g. k-ε class), originally developed for single-phase non-cavitating flows, have a tendency to over-predict the turbulent viscosity at the closure of cavity and its downstream region. It has been suspected that the inherent unsteadiness of sheet cavitation is significantly dampened by the viscosity and the models are hardly able to capture the shedding dynamics. The deficiency of the standard turbulence models deserves more attention as the above-mentioned tendency is not just associated with one specific RANS solver or one specific cavitation model. Studies were also reported in [6]-[10][12][18][19].

In our previous work [13], a modification of turbulent viscosity was implemented in a RNG k-ε model following the idea of Reboud et al.[6]. This led to a fairly good prediction of re-entrant jets and shedding of cloud cavities on a 3D twisted hydrofoil when compared with the experiment data [3]. The study indicates that the turbulence modelling may have an important role for cavitation predictions. A lesson learned from the two workshops in the EC project VIRTUE is that not only the cavitation model but also the turbulence model, the implementation and numerical treatment of equations have significant influence on results. Recently, the success of the LES method [15] in capturing the rich detail of small-scale flow structures in cavitating flows demonstrates from a different perspective the important role of *turbulence handling* in the cavitation prediction.

The paper presents a study of using a modified SST k-ω model to predict the steady and unsteady cavitating flows around 2D and 3D hydrofoils with a multi-phase mixture flow RANS method. For non-cavitating turbulent flows, it is known that SST k-ω turbulence model has better performance over k-ε models for wall-bounded boundary layer flows under adverse pressure gradient and separation, as reported for example in the last two international CFD workshops on ship hydrodynamics [25][26] and several propeller flow simulations. Since we have been using the model for propeller flow simulations with success, it is of practical interest and significance to investigate its capability to predict cavitating flows and the performance breakdown due to cavitation. The aim of the present work is to study the feasibility of a *modified* SST k-ω model to predict the stable and fluctuating sheet cavitation on hydrofoils. For 2D foils the mass transfer due to cavitation is modeled by Schnerr-Sauer's cavitation model [16] available in the recent release of ANSYS FLUENT 12.0. For the 3D foil, Singhal's full cavitation model is used.

Two hydrofoils are studied. The first one is a 2D NACA0015 foil having a 6° angle of attack and operating in a 6m/s uniform flow at two cavitation numbers, σ=1.6 and σ=1.0. This is intended to test the basic behavior of the model in steady and unsteady cavitating conditions. For the 2D foil, comparison will be made between the standard and the modified SST model, as well a comparison with available experiment data.

The second hydrofoil is the Delft 3D twisted foil operating in a 6.97m/s uniform flow and at σ=1.07. The study is oriented to realistic situations with more complicated cavitation and vortex structures. The foil is characterized with a periodic shedding of a large-scale primary cavity and small secondary cloud structures according to the experiment observation [3]. The strong interaction of re-entrant jets and the complex shed structures have made the case a great challenge for numerical simulations of 3D unsteady sheet/cloud cavitation.

NUMERICAL METHODS AND MODELS

Multi-phase model
The multi-phase mixture model in FLUENT12.0 assumes that the working medium is a single fluid with a homogeneous mixture of two phases (liquid and vapor). Therefore, only one set of RANS equations is solved for the mixture fluid. Denoting the density of the mixture fluid by ρ_m, the continuity equation for the mixture flow becomes:

$$\frac{\partial}{\partial t}(\rho_m) + \nabla \cdot (\rho_m \vec{v}_m) = 0 \tag{1}$$

The momentum equation for the mixture reads:

$$\frac{\partial}{\partial t}(\rho_m \vec{v}_m) + \nabla \cdot (\rho_m \vec{v}_m \vec{v}_m) = -\nabla p + \nabla \cdot \left[\mu_m \left(\nabla \vec{v}_m + \nabla \vec{v}_m^T \right) \right] + \rho_m \vec{g} + \vec{F} \tag{2}$$

The density constitution of each phase in a mixture-flow cell is described by means of a scalar volume fraction. The relation between different volume fractions is linked by:

$$\rho_m = \alpha_v \rho_v + (1 - \alpha_v) \rho_l \tag{3}$$

where α_v and α_l are the volume fraction of vapor and liquid respectively. To close the equations an additional transport equation is solved for α_v. To account for the mass transfer between phases a cavitation model is needed, as discussed below.

Cavitation model
The cavitation model used for 2D foil is developed by Schnerr and Sauer [16]. It solves for the vapor volume fraction with the following transport equation:

$$\frac{\partial}{\partial t}(\alpha_v \rho_v) + \nabla \cdot (\alpha_v \rho_v \vec{v}_m) = R_e - R_c \tag{4}$$

The source terms R_e and R_c were derived from the bubble dynamics equation of the generalized Rayleigh-Plesset equation and account for the mass transfer between the vapor and liquid phases in cavitation. They have the following form:

$$R_e = \frac{\rho_v \rho_l}{\rho_m} \alpha(1-\alpha) \frac{3}{\Re_B} \sqrt{\frac{2}{3} \frac{(p_v - p)}{\rho_l}} \tag{5}$$

when $p_v > p$, and

$$R_c = \frac{\rho_v \rho_l}{\rho_m} \alpha(1-\alpha) \frac{3}{\Re_B} \sqrt{\frac{2}{3} \frac{(p - p_v)}{\rho_l}} \tag{6}$$

when $p_v < p$. The bubble radius R_B can be determined by:

$$\Re_B = \left(\frac{\alpha}{1-\alpha} \frac{3}{4\pi} \frac{1}{n_0} \right)^{1/3} \tag{7}$$

where n_0 is the bubble number density. A default value $n_0 = 10^{13}$ is used here. Note that for this cavitation model the non-condensable permanent gas is not accounted for.

Singhal's cavitation model is referred to [17].

Turbulence model

The SST k–ω model in FLUENT is due to Menter [14]. The formulation and the model constants for k and ω equations are unchanged in the present method. Instead, a modification is made to the formula for turbulent viscosity μ_t following the idea of Coutier-Delgosha and Reboud et al. [8],

$$\mu_t = f(\rho)C_\omega \frac{k}{\omega}, \tag{8}$$

$$f(\rho) = \rho_v + \frac{(\rho_m - \rho_v)^n}{(\rho_l - \rho_v)^{n-1}}, \text{ where } n > 1 \tag{9}$$

The function $f(\rho)$ in Eq. (8) has replaced ρ_m in the standard formula and C_ω represents all the remaining terms in the standard formula. As can be seen in Eq. (9), for cavitating flow $f(\rho)$ will reduce the turbulent viscosity in regions with high vapour volume fraction, whereas for non-cavitating liquid flows it returns to the original formula. The exponent n was set to 10, the same as used in [8]. To distinguish the difference, we denote the model using the modified μ_t as the **modified** SST, whereas the model using the original formula for μ_t as the **standard** SST. The modification is realised via a UDF (user defined function) that is compiled and linked to the solver.

The second order QUICK scheme is used for convection terms in all equations for all cases. A fully coupled solver (for the 2D NACA0015) or the SIMPLE (for the 3D twist foil) scheme is used to solve pressure and momentum equations. The time step is 5e-4(s) and 20 iterations are run within each time step.

GRIDS AND INFLOW CONDITIONS

2D NACA 0015 foil

The flow and boundary conditions for NACA0015 foil were adopted from the second VIRTUE-WP4 Workshop. The foil is 0.2m long in chord and located in the middle of a 0.57m high rectangular tunnel. The inlet plane of the computational domain is located at 2 chord length upstream the leading edge and the outlet plane at 4 chord length downstream the trailing edge. The foil has a 6° angle of attack (AoA) and is operated at two representative cavitation conditions, (a) σ=1.6 (cavity expected to be stable) and (b) σ=1.0 (cavity expected to be unsteady and shedding). Table 1 gives the flow and boundary conditions. The physical properties for the liquid and the vapor in Table 1 correspond to a water temperature at 24 ℃ and these values have been used for all the 2D and 3D cases. It can be mentioned that the liquid-vapor density ratio at this temperature is as high as 43391:1.

Three geometrically similar hexahedral grids are generated to study the grid sensitivity of solution. Figure 1 shows the coarse grid. More grid information can be found in Table 2.

Table 1   Flow and boundary conditions for NACA 0015

Boundary Conditions	Values	
Upstream: constant velocity inlet, [m/s]	6.0	
turbulent intensity [%]	1	
turbulent viscosity ratio [-]	8	
Downstream: pressure outlet, [kPa]	31.7 for σ=1.6, 20.9 for σ=1.0	
Foil surface: No-slip	-	
Tunnel wall: Slip	-	
Physical properties of water	**Vapour**	**Liquid**
Vaporization pressure, [kPa]	2.97	
Dynamic viscosity, [kg/ms]	9.95×10^{-6}	0.00110
Density, [kg/m^3]	0.023	998.0

Table 2   Information on grids for NACA 0015

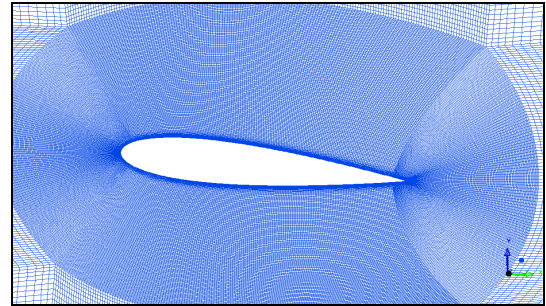| Grid	# Cells	Size variation	level
G3	35030	2.0h	coarse
G2	62386	1.5h	medium
G1	140120	1.0h	fine

Figure 1: The coarse grid G3 for NACA0015 foil
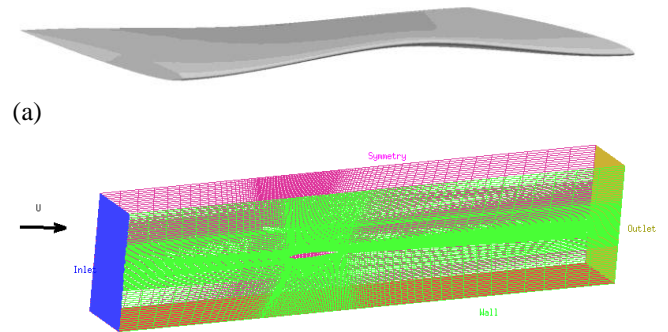

(a)

(b)
Figure 2: (a) geometry of 3D twisted hydrofoil; (b) the computational domain

3D Delft twisted hydrofoil

The Delft twisted hydrofoil is a rectangular wing (0.15m chord and 0.3m span) with a NACA0009 profile, **Figure 2**(a). The foil is twisted along the spanwise direction to give a maximum angle of attack 9° at midspan section and -2° at the tunnel wall. Thus the cavitation develops mainly on the suction side mid-span area. The foil is operated at σ=1.07 in the tunnel

with a freestream velocity 6.97m/s. The tunnel has a 0.3m by 0.3m cross section. The inlet plane of the computational domain is located at 2.0 chord length upstream the leading edge and the outlet plane at 4.0 chord length downstream the trailing edge. Table 3 gives the flow and boundary conditions.

An O-H type grid is generated for the domain with sufficient refinement ($y^+ \approx 1$) towards foil surface, **Figure 2**(b). The grid has about 1044 000 cells.

Table 3   Flow and boundary conditions for 3D twist foil

Boundary Conditions	values
Upstream: constant velocity inlet, [m/s]	6.97
turbulent intensity [%]	2
turbulent viscosity ratio [-]	10
Downstream: pressure outlet, [kPa]	29.0
Foil surface: No-slip	-
Tunnel wall: Slip	-

RESULTS AND DISCUSSION

(A) 2D NACA 0015 foil at non-cavitating condition

Steady non-cavitating flows are first computed for all three grids to check the grid sensitivity and the performance of the fully-coupled solver of FLUENT 12. The pressure coefficient (Cp) distribution over the foil is shown in **Figure 3**. Three grids yield very close Cp distributions, except a minor deviation of Cp_{min} and Cp_{max} near the leading edge. This is more clearly seen in Table 4, where the C_L and C_D for the three different grids differ only in the 4th decimal slightly, and they are in close agreement with the measured C_L and C_D. Results of Cp_{min} and Cp_{max} in Table 4 are also fairly close to each other for different grids. For steady non-cavitating flow, it appears that even the coarse grid G3 does a good job. However, we will see below that greater difference in results does exist for different grids when it comes to cavitating flows.
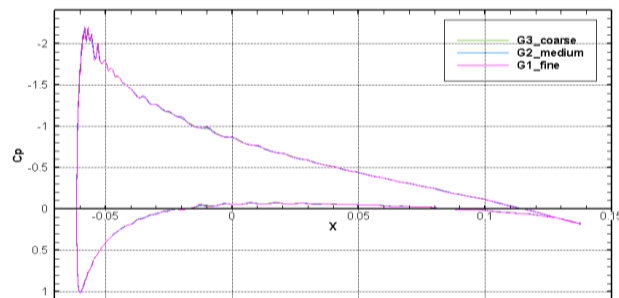

Figure 3: Pressure coefficient Cp by three different grids

Table 4   Lift/drag coefficients by different grids

Grid #	C_L	C_D	Cp_{min}	C_{pmax}
G3	0.677348	0.013840	-2.1637	1.0079
G2	0.677162	0.013818	-2.1945	1.0103
G1	0.677204	0.013785	-2.1994	1.0114
Exp.	0.660 ±5%	0.014 ±14%	-	-

(B) 2D NACA 0015 foil at σ=1.6

At this condition, the partial cavity developed on the foil is expected to be quasi-steady. Using the standard SST model, solution does lead to a very stable and attached sheet cavity near leading edge for grid G3 and G1, as shown in **Figure 4**. On the other hand, with the modified SST model, the predicted sheet cavity shows a different extent of fluctuation for different grids. For the coarse grid G3, only the rear part of cavity reveals very little fluctuation (**Figure 5**), whereas for the fine grid G1, the cavity is oscillating at a rather high frequency, with a periodic shedding of a small cavity at the trailing edge, four instants of this cycle is shown in **Figure 6**. A slightly longer sheet is obtained with the modified SST model, and the finer the grid the longer the sheet, **Figure 5** vs. **Figure 6**. Nonetheless, the modified SST model never leads to a large-scale shedding at this condition.
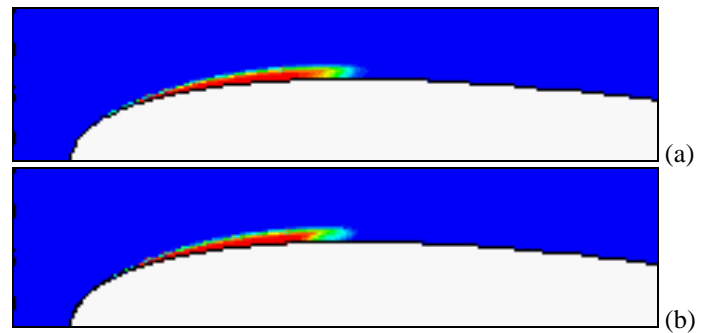

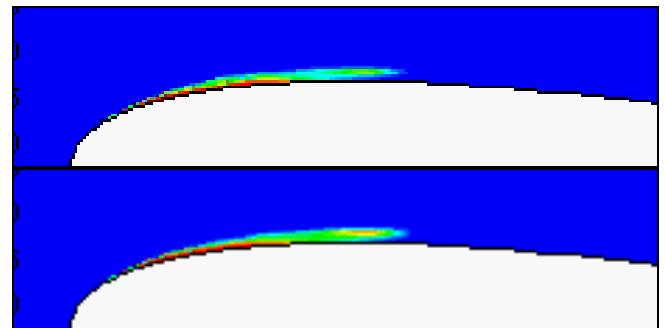**Figure 4:** Cavity shape for σ=1.6 on grid G3 (a) and fine grid G1 (b), by the standard SST model

Figure 5: Cavity shape at σ=1.6, by grid G3 and the modified SST model

The oscillation is also reflected clearly in **Figure 7** (a) showing the time history of variation of total vapor volume, and in **Figure 7** (b) showing the variation of lift coefficient C_L for grid G1. The total vapor volume oscillates around a mean value about 5e-5 (m^3) and never ceases to zero, indicating the presence of a sheet cavity all the time. The C_L value varies more violently with some high-peak amplitudes, the behavior is known for the Schnerr-Sauer's model and was also reported by others [15][23]. It will be discussed more for computations at σ=1.0.

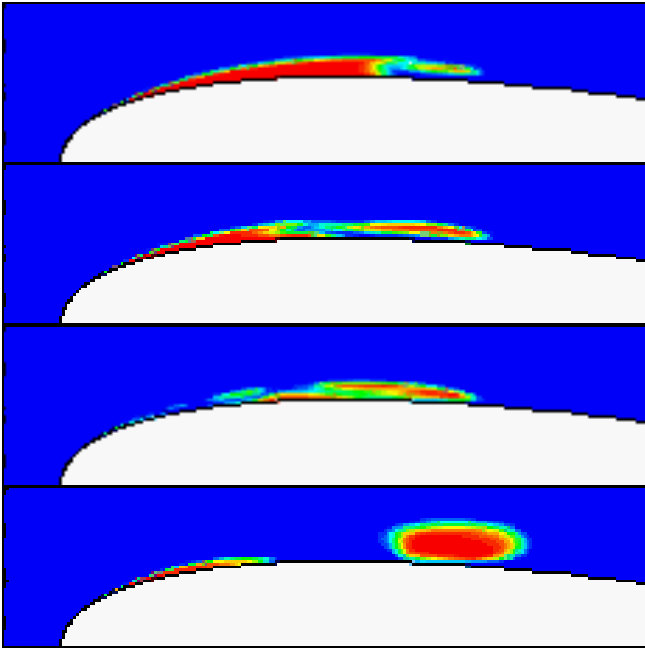**Figure 6:** Cavity at σ=1.6, by grid G1 and the modified SST model

The oscillation frequency based on the total vapor volume is about 32Hz, whereas the C_L curve exhibits a multiple frequency domain with the first three being 34Hz, 66Hz and 100Hz respectively. As cavitation is always unsteady in nature, some extent of unsteadiness is expected to be natural also for σ=1.6. This character seems to be reflected by the modified SST model but not captured with the standard SST model.

The time-averaged C_L and C_D for different turbulence models on grid G1 can be found in **Figure 19** in comparison with the relevant experimental data by Kjeldsen et al. [20]. As seen in the figure for σ=1.6, the C_L predicted by the modified SST has better agreement with the data than the standard SST. The C_D given by the two models are nearly the same.
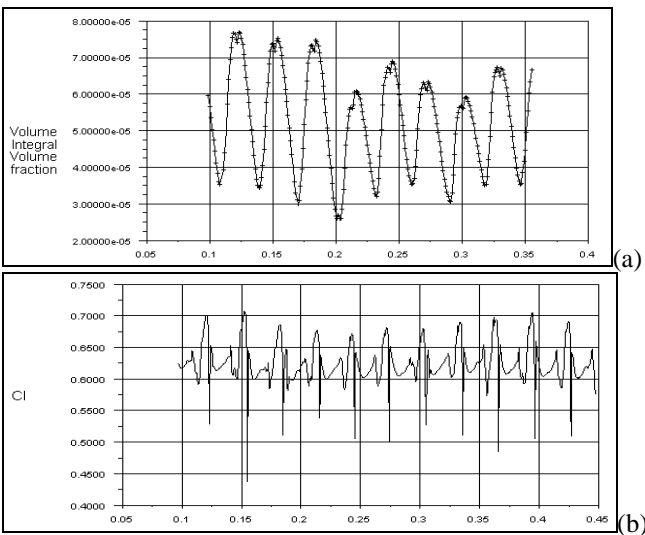

Figure 7: (a) Total vapor volume variation, ~32Hz; (b) Time history of C_L for σ=1.6 on grid G1, by modified SST

(C) 2D NACA 0015 foil at σ=1.0

The cavitation under this flow condition is expected to be highly unsteady, fluctuating and shedding. Significant difference in results is noted for the standard and the modified SST model.

Results predicted by the standard SST model

During the calculation it is seen that the predicted cavity performs a few initial back-forth oscillation, then retreats back to the leading edge and finally becomes a stable attached sheet. Most noticeably, there is no shedding at the rear of the cavity. The tendency is very similar for grid G3 and G1, see Figure 8.

Like the standard RNG k-ε model we studied in [13], the failure of the standard SST model in predicting the dynamic shedding of unsteady sheet cavity is likely caused by an unrealistically high eddy viscosity downstream the cavity region that dissipates out the inherent unsteadiness of the flow, as will be shown below.
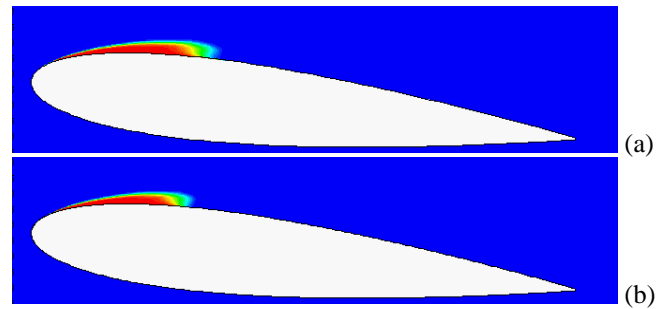

Figure 8: Vapor void fraction, showing a quasi-steady sheet cavity for NACA15 at σ=1.0 on grid G3(a) and G1(b), by standard SST

Turbulent quantities predicted by the standard SST model

To highlight the problem that the standard turbulence model is encountered in predicting the unsteady cavitation, the turbulent kinetic energy k predicted by the *standard* SST model under the non-cavitating and a cavitating condition (σ=1.0) is shown in Figure 9. The turbulent viscosity ratios (v_r) under the same conditions are given in Figure 10. The results from the fine grid G1 are also included to show the effect of grid refinement. The cavity shape relevant to these conditions is referred to Figure 8.
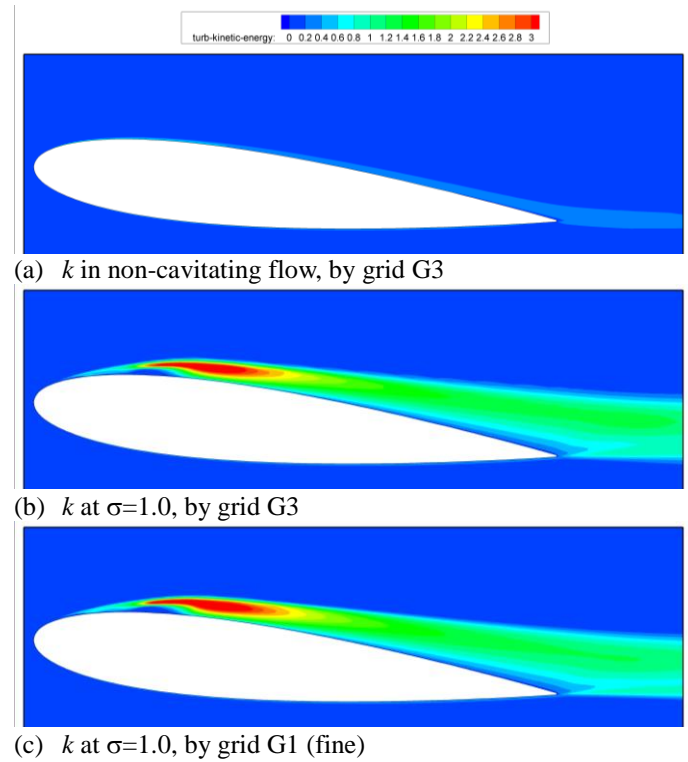
Comparing the k distribution in Figure 9 (b), (c) and (a), we see that there is a high concentration of k right behind the cavity closure region in Figure 9(b) and (c). Moreover, the high level of k extends all the way downstream on the remaining part of the foil. Comparing the v_r distribution in Figure 10 (b), (c) and (a), it is clear that the turbulent viscosity level in cavitating conditions is unrealistically too high (in the order of 5~10 times larger than in the non-cavitating case). There is no reason to believe that in the region downstream a sheet cavity the v_r should be considerably larger than the corresponding non-cavitating case. On the contrary, the turbulent viscosity level is expected to be somewhat lower due to the compressibility effects in the local mixture-phase regime that decrease the turbulence level and Reynolds stresses. It is very likely that the high turbulent viscosity in this region has suppressed the natural instabilities of the unsteady cavitation and prevents the solver to capture the shedding.

(a) k in non-cavitating flow, by grid G3

(b) k at σ=1.0, by grid G3

(c) k at σ=1.0, by grid G1 (fine)

Figure 9: (a) turbulent kinetic energy k for the non-cavitating flow, compared with cavitating flow on two grids, (b) and (c)

(a) v_r in non-cavitating flow, by grid G3

(b) v_r at σ=1.0, by grid G3

(c) v_r at σ=1.0, by grid G1 (fine)

Figure 10: (a) turbulent viscosity ratio v_r for the non-cavitating flow, compared with cavitating flow on two grids, (b) and (c)

It is also seen in Figure 10(c) that even with the fine grid G1 (twice denser), the v_r is only slightly decreased. Therefore, the large value of v_r can hardly be attributed to just a grid resolution issue.

As a first remark, the tendency to produce unrealistic turbulent viscosity is not only associated with the standard SST model. Similar behaviour has been found in our previous work for the RNG k-ε and a low-Re k-ε model in FLUENT. Such behavior of standard k-ε or k-ω models was also observed in other studies [6]-[10] and [12] where completely different RANS solvers and different cavitation models were used. Thus it is a common issue not solely related to FLUENT.

The second remark is on the huge water-vapor density ratio d_r $(=\rho_l/\rho_v)$ involved in cavitating flows. A realistic density ratio (over 43000:1) has been used in all the calculations. The large density ratio means a sudden change of mixture density ρ_m across the cavity interface. It is suspected that the large density ratio may have introduced some unwanted numerical effects when solving the k and ω equations, and thereby resulted in unrealistically high turbulent viscosity.

The above results highlight the problem that existing turbulence models may face in predicting unsteady cavitating flows, and emphasize the need for further research on the interaction effects between cavitation and turbulence, as well as the turbulence modeling for cavitating flows.
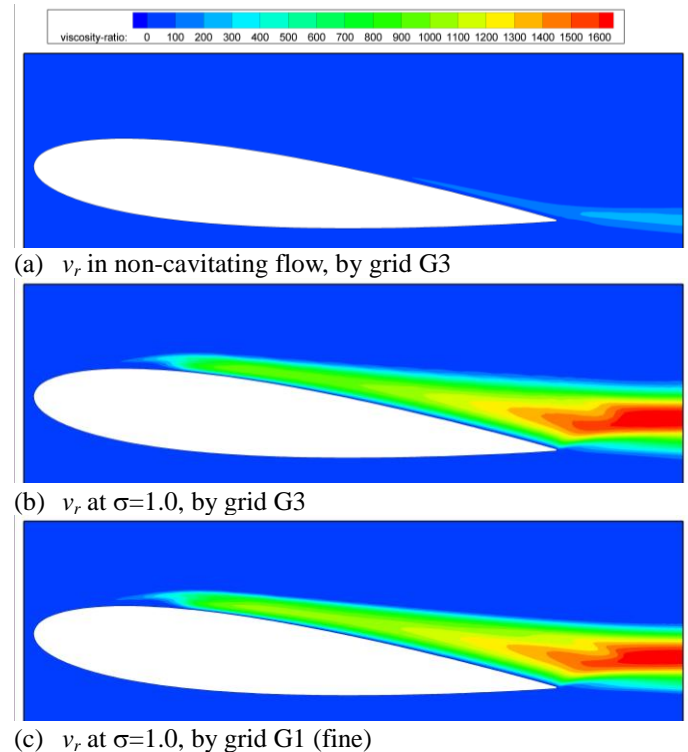
Results predicted by the modified SST model

The discussion below will concentrate on the results obtained with the modified SST model on the fine grid G1, unless mentioned otherwise. With the modified SST model, the results reveal a periodic shedding of large structures and small cavitating vortices. In general, two different shedding behaviors are observed. (1) Shedding of medium to large scale cavities; (2) Shedding of a series of small cavitating vortices downstream an upstream moving sheet cavity. They are discussed below.

(1) Shedding of medium to large structures

Figure 11 displays eight sequences of a shedding cycle. The development of re-entrant jet moving upstream and the cavity break-off are clearly visualized in the figure.

The development of re-entrant jet inside the sheet cavity can be identified again from the velocity vectors in **Figure 12** in three sequences, corresponding to the frame (c), (d), and (e) of Figure 11 respectively. This re-entrant jet appears to be thin, strong and quite durable, such that it can pinch off a cavity at about 1/4 chordwise location first (frame (d)), then it continues to travel towards the front of the remaining cavity, finally finishes the second break-off near the leading edge, frame (e). The two cloudy-like shed cavities are then rolled up together and transported downstream, frame (f)-(h) in Figure 11. This kind of the shedding is mainly caused by the upstream moving re-entrant jet and its interference with the external flow. An effect called "shear by filling the sheet with internal jets" according to Bark et al.[1].
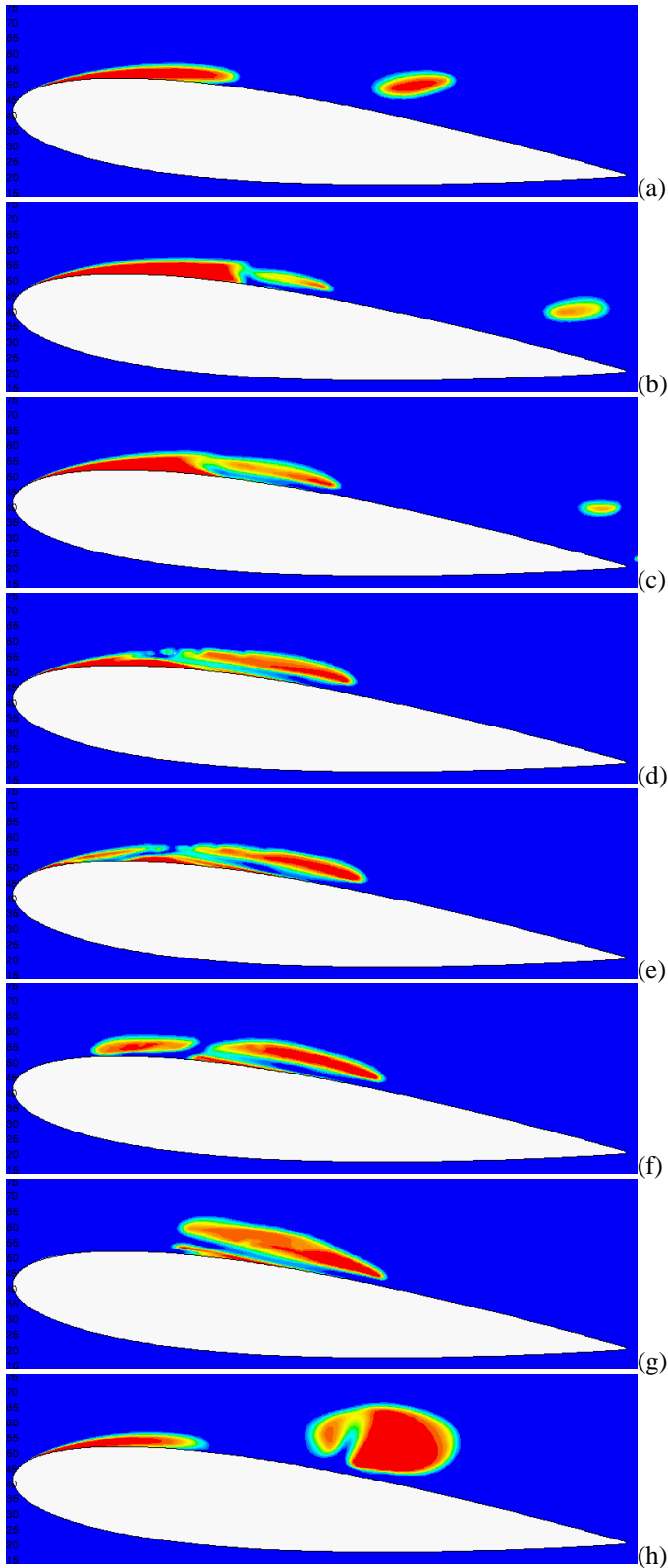
Figure 11: Cavity shape expressed by vapor void fraction at σ=1.0, showing sequences of the shedding and break-off. Color scale: red=pure vapor, blue=pure liquid.
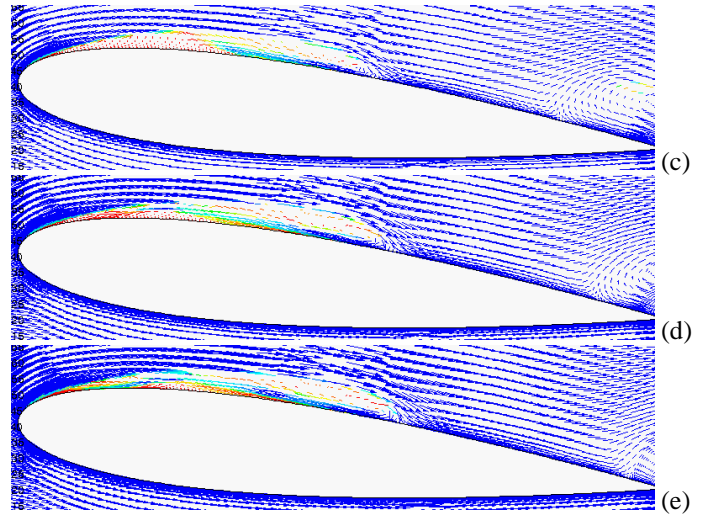

Figure 12: Velocity field corresponding to the sequence (c), (d) and (e) of Figure 11. Color scale: blue for pure liquid; red for pure vapor

(2) Shedding of a series of cavitating vortices

Eight sequences of such a cycle are shown in **Figure 13**, and the corresponding velocity field is plotted in **Figure 14**.

The process starts with development of a long and thick partial cavity with an "open" closure region and without any noticeable re-entrant jet, frame (b). Due to possibly downstream disturbance of previously shed cavities, it starts to shed a vortex cavity, frame (c). Note that this shed vortex cavity does not transport downstream immediately. Instead it remains at the same chordwise location for quite some time (from frame (d) till frame (g) in **Figure 13**) and becomes *cloudy* in frame (f)-(g). During the same period, the attached sheet cavity performs a fast upstream collapse. Meanwhile two new vortex cavities are shed from the trailing edge of the upstream moving sheet cavity, frame (d) to (g).

From the velocity vectors in **Figure 14** (c)-(e), it is seen that there is a sustainable reversed flow attempting to penetrate through the cavity at closure region. The reversed flow is likely induced by the first-shed vortex that stays in the same location and functions here like a re-entrant jet. The locally strong pressure gradient, the interaction with the shed vortices and the reversed flow at the closure region are considered to be the likely cause of the shedding of a number of vortex cavities.

This shedding behavior is to some extent similar with the LES simulations presented by Chalmers University at the 2nd VIRTUE-WP4 workshop at the same conditions. Of course, the RANS cannot predict so much coherent flow structures as LES. The RANS predicted internal flow inside the sheet cavity is often found to be less pronounced than that by the LES.
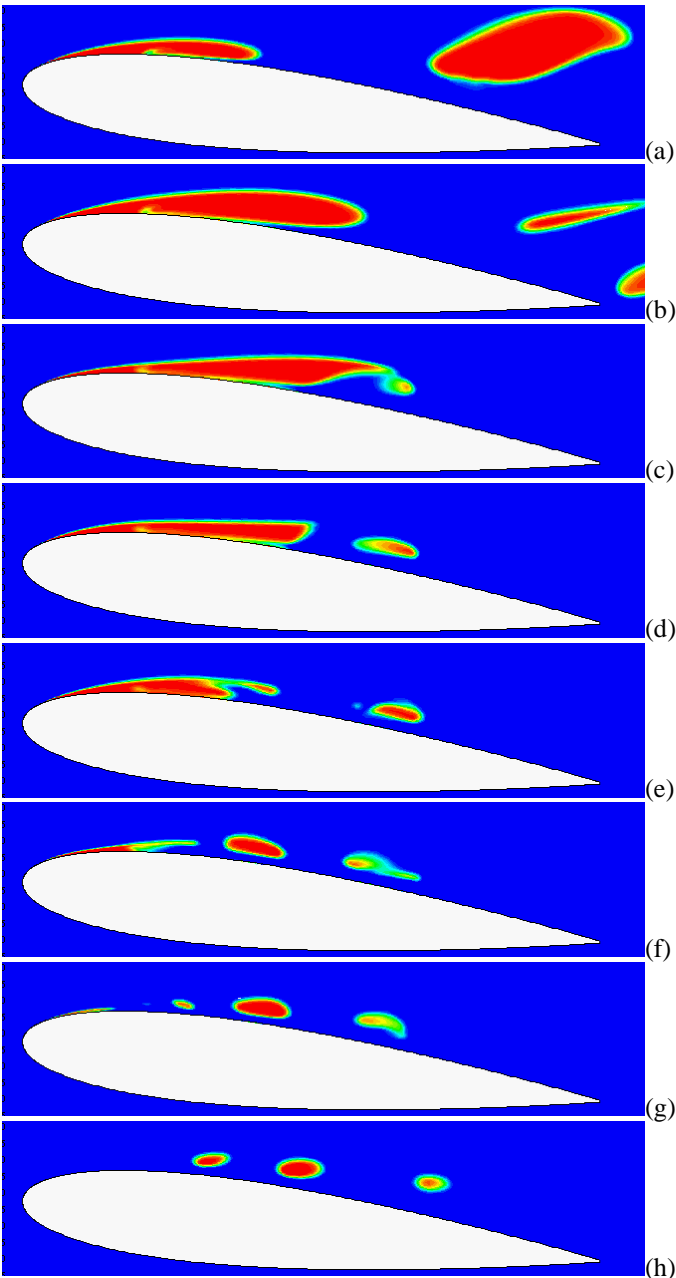
7

Figure 13: Shedding of cavitating vortices from an upstream moving collapse sheet. Color scale: red=pure vapor, blue=pure liquid.

The shedding of a series of vortex cavities observed here has a similarity with a special type of "secondary cavities" termed by Bark et al [1] as "vortex group cavitation". Existence of such type of cavitation was observed first in the EROCAV project [2] and was reconfirmed in a recent experiment at SSPA [22][1]. Three images of a high-speed video recording from the experiment are shown in **Figure 15** to give an idea of its development and cloudy look. The significance to identify this kind of shedding in CFD simulations is that it represents a type of cavitation that can be potentially erosive for propellers and hydrofoils [1]. Therefore a well-established CFD method or solver should not ignore or miss to capture this phenomenon.
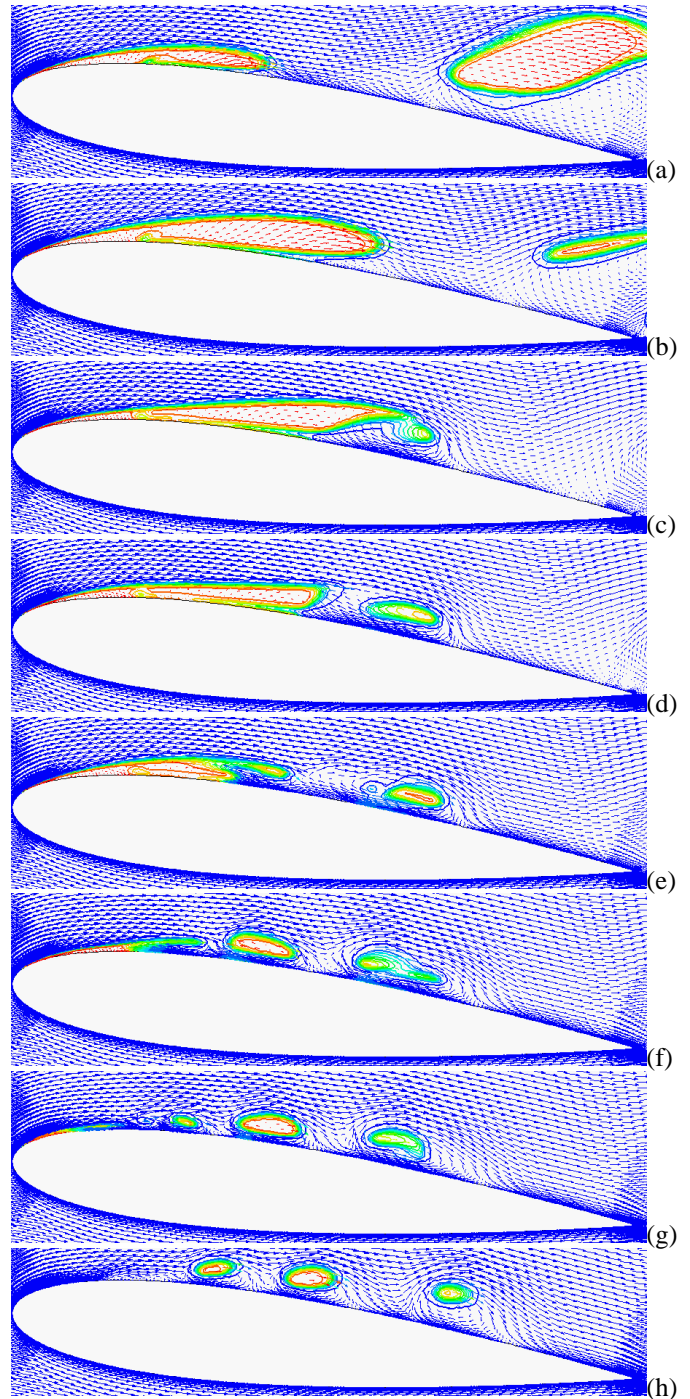

Figure 14: Velocity field corresponding to the sequences in **Figure 13**. Color scale: blue for pure liquid; red for pure vapor. Contour lines of vapor volume fraction are also plotted.

Figure 15: The potentially erosive vortex group cavitation shed downstream an upstream collapsing sheet near the root of a propeller (leading edge on the left). Experiment carried out in SSPA's cavitation tunnel [22].

The time history of the lift coefficient C_L is depicted in **Figure 16** for grid G3 and G1. The unrealistic spikes of C_L–curve in the figure is a known behavior of Schnerr-Sauer's cavitation model, which generates an instantaneously sudden change of pressure (or pressure wave) field during the transient simulations. This unphysical behavior of the model has also been observed and reported by the participants [15][23] who used the model in the 2nd VIRTUE-WP4 workshop.

The time evolution of the integrated vapor volume is shown in **Figure 17** for grid G3 and G1. It can be derived from the graph that the integrated cavity volume predicted by the fine grid G1 is somewhat smaller than G3. Furthermore, the shedding of small scale vortex cavities was not well captured with the coarse grid G3.

The shedding frequencies based on the lift coefficient and the vapor volume variations are given in **Figure 18** (a) and (b) for grid G1. Both signals reveal that the shedding occurs at three main frequencies. As can be read from the figure, the first two frequencies (~3.5Hz and ~9.1Hz) obtained from the lift and the vapor volume variations are nearly identical. The third frequency is slightly different: 16.3Hz from the lift coefficient signal and 13.5Hz from the vapor volume variations. The third frequency (in between 13.5 and 16.3Hz) seems to fall into the frequency band of the experiment value (~16.0Hz) at this condition. However, the most dominant frequency in the simulations is the lowest one (3.5Hz), which was not reported in the experiment. Further analysis is needed to sort out the discrepancy. As to the grid sensitivity on shedding frequency, without showing detail it can be mentioned that three similar frequencies but with slightly lower values are obtained with the coarse grid G3. Here again, we notice that finer grid is needed for cavitation predictions.

Finally, the time-averaged lift and drag coefficients, C_L and C_D are compared with the relevant experiment data by Kjeldsen et al.[20] in **Figure 19**. Note the minor difference in AoA between the data (measured at $\alpha=5°$ and $\alpha=7°$) and the computations ($\alpha=6°$). It can be seen that the C_L and C_D predicted by the modified SST model (solid symbols in magenta) have better agreement with the measured data than those by the standard SST model (solid symbols in green). Common for models, the predicted C_L and C_D values at $\sigma=1.0$ is considerably lower than the data, whereas the agreement with measured C_L at $\sigma=1.6$ and at the non-cavitating condition is reasonably good. The large discrepancy at $\sigma=1.0$ is probably dependent on both the cavitation model and the turbulence model, as the standard SST k-ω model also gives a poor prediction at $\sigma=1.0$, so the discrepancy with experiment is not likely caused by the introduction of eddy viscosity modification.
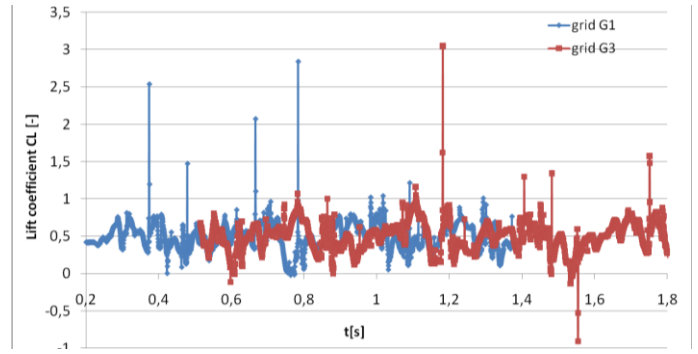

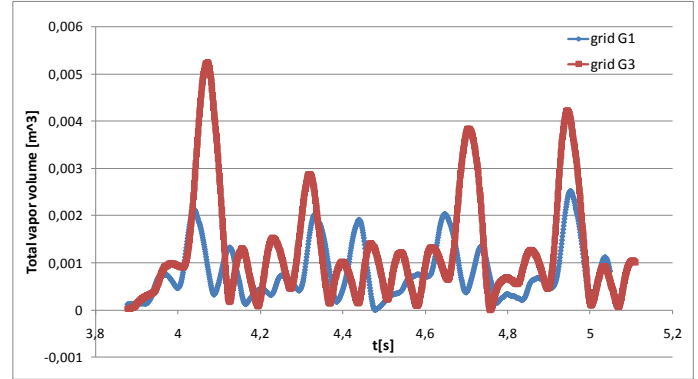**Figure 16:** Variation of lift coefficients, $\sigma=1.0$, modified SST model

Figure 17: Variation of total vapor volume with time, $\sigma=1.0$, modified SST model
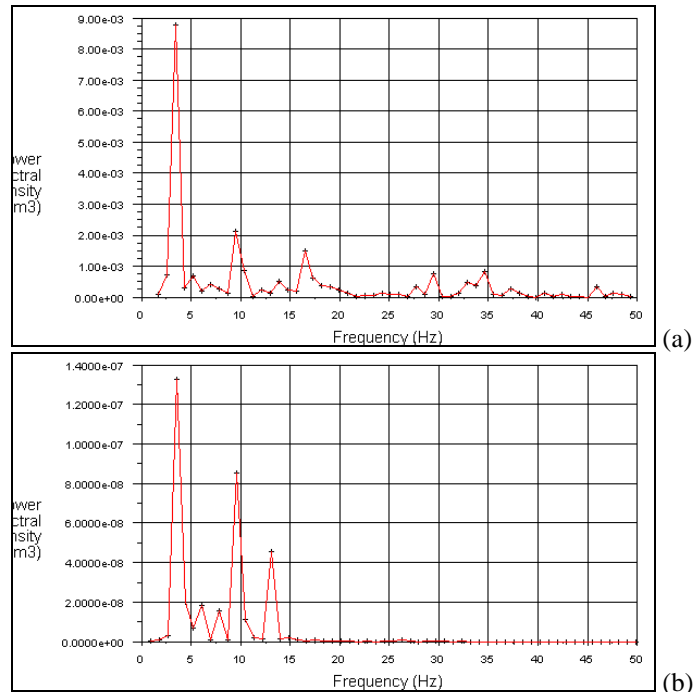

Figure 18: Shedding frequencies based on (a) lift coefficient variations; (b) integrated vapor volume at $\sigma=1.0$, predicted on grid G1 with modified SST model
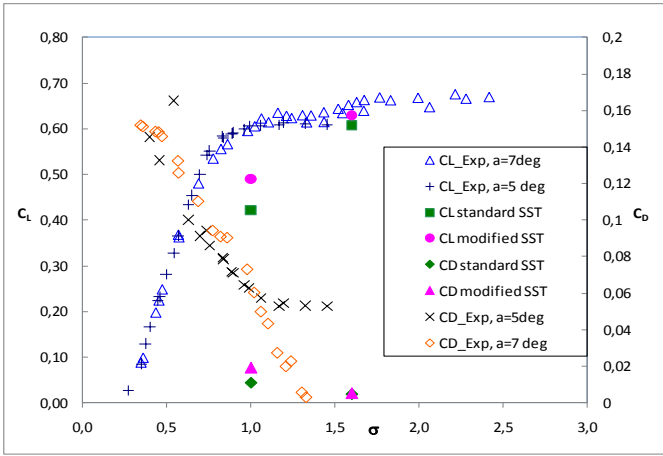
Figure 19: Comparison of C_L and C_D with the data at two nearby AoA. Experiment data by Kjeldsen et al.[20]

(D) 3D Delft twisted foil at σ=1.07

The 3D Delft twisted foil proves to be a challenge case for RANS simulation. When the modified SST k-ω model together with Schnerr-Sauer's cavitation model was applied to the case, it was found that the modification was not effective enough to bring down the turbulent viscosity. Consequently only a very limited shedding of small cavities occurred at the closure, and the predicted cavity length was much shorter than the experimental one. The behavior was found the same for a fine grid. It appears that another model constant (exponent *n*) is needed in Eq. 9 for the 3D foil.

Instead of changing the exponent *n* in Eq. 9, it was decided to keep exactly the same modified SST model as used in the 2D cases, but combine it with the *Singhal's cavitation model* [17]. The results presented below are obtained with this model combination. Although they are not related to the Schnerr-Sauer's model, they are relevant to the topic of the paper. The mass fraction of non-condensable gas in Singhal's model is set to 2.0e-6.

For the 3D twisted foil, the cavitation computed by the standard SST model turns into a stable attached sheet with a length much shorter than the measured one (Figure 20). The reason for such a result is similar to what has been discussed for the 2D NACA0015 foil. It can be seen in Figure 21 where an unrealistically high eddy viscosity region is developed over nearly the entire suction side surface. In this case too, the eddy viscosity is found to be higher than that in the non-cavitating case, showing that the problem with the standard turbulence model is present also in the 3D case.
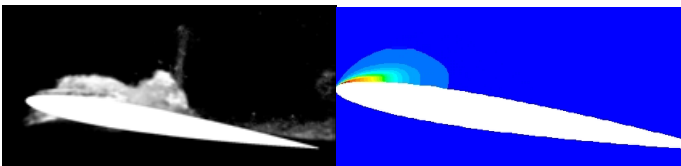

Figure 20: Left: photo of maximum extension of cavity at the mid-span section plane. Right: vapor volume fraction showing the maximum extension of a quasi-steady attached sheet cavity predicted by the standard SST model
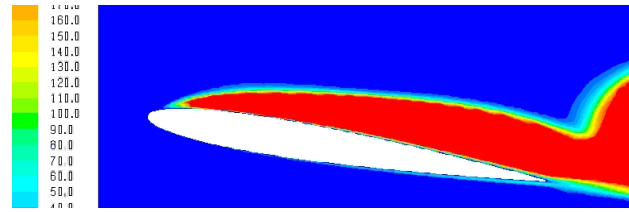

Figure 21: The eddy viscosity at the mid-span section plane, computed by the standard SST model

In contrast with the standard model, the modified SST model results in shedding of large cloud structures fairly similar to those observed in the experiment. Seven sequences of a shedding cycle are shown in Figure 22, with the video images on the left and the iso-surface of $α_v$=0.1 on the right column. The limiting streamlines visualize the directions of the internal jets (re-entrant and side entrant jets). The break-off, shedding and transport of the primary cavity can be seen clearly in Figure 22. More description of cavitation development for this particular 3D foil is referred to our previous work in [13].

Figure 23 compares the experimentally observed and the predicted cavity development in one cycle at the mid-span section plane. The experiment images are taken from one cycle at equal time intervals. The computational results are also taken from one cycle but not at exactly identical time intervals. As seen from these sequences, the computed shed cavities that are transporting downstream are somewhat smaller than the experiment ones whereas the computed attached cavity seems agree well with the experiment. The maximum length of the attached cavity is about 0.4C (C=chordlength) and the experimental value is ~0.45C. The time-averaged C_L is approximately 0.44, to be compared with the measured value of 0.51 from [3].

The time variation of the total vapor volume is shown in **Figure 24**(a), whose spectrum analysis reveals three main frequencies, 2, 8 and 14Hz respectively, **Figure 24**(b). The dominant frequency (14Hz) is about 33% lower than the experimentally observed shedding frequency (~21Hz).

Results so far justifies that the modified SST model can improve the RANS solver's capability to predict the essential features like re-entrant jets and shedding of large scale cloud structures for this particular 3D foil.

CONCLUDING REMARKS

In the present study we observe that the standard SST *k–ω* model produces an unrealistically high level of turbulent viscosity for cavitating flows, and the high viscosity is likely the reason for the model to fail to capture the dynamic behavior of unsteady sheet/cloud cavitation. Similar behaviour has been found in our previous work with the RNG k-ε and a low-Re k-ε model available in FLUENT. The observation is in line with the findings of the turbulence model behavior in [6]-[10],[12],[18]-[19] where different RANS solver and different cavitation models were involved, showing this being an unsolved problem of common interest.

The grid refinement improves the resolution of the flow but is still unable to reproduce the experimentally observed shedding dynamics when using the standard SST *k–ω* model.
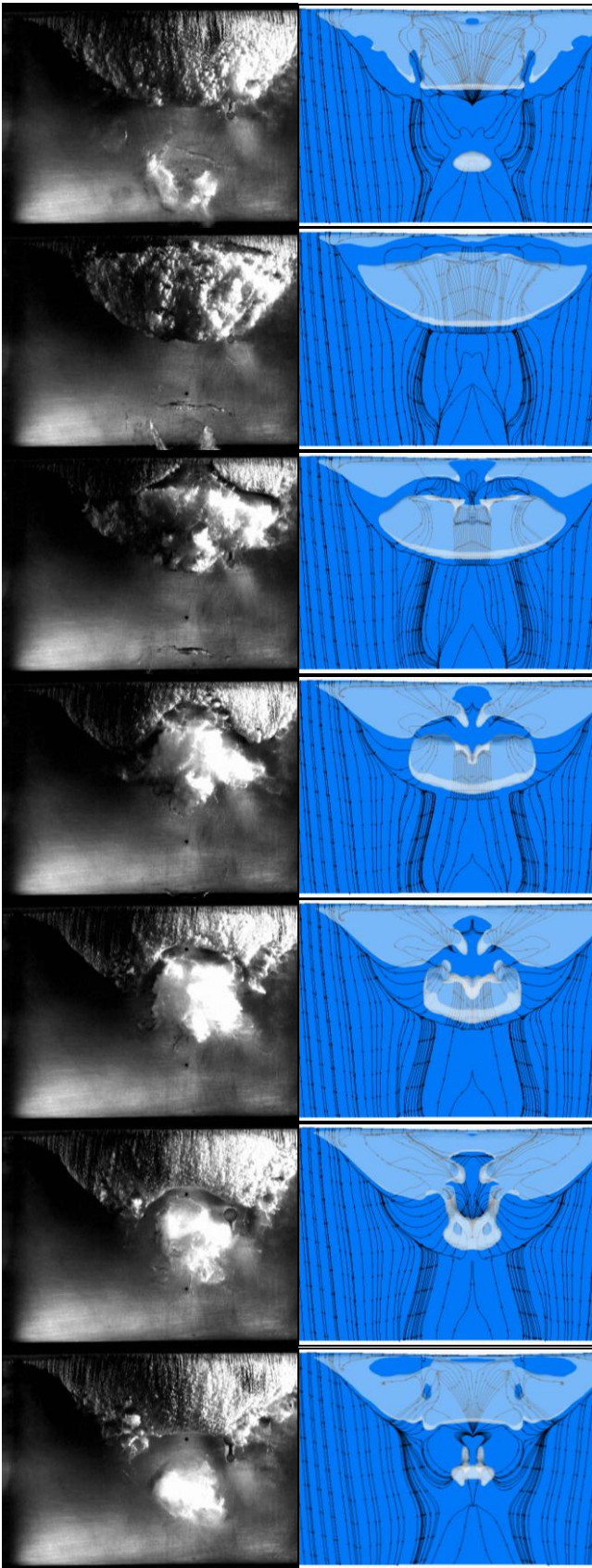
Figure 22: Sequences of cavity image [3] (left) vs. isosurface of vapor void fraction at α_v=0.1 together with the limiting streamlines, flow from top to bottom, by modified SST model

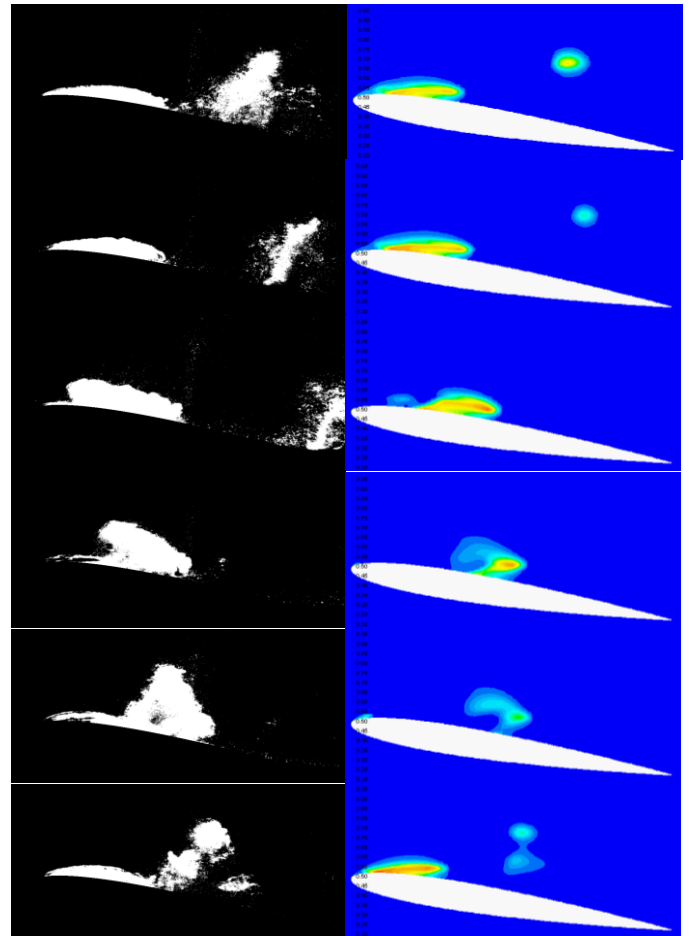**Figure 23:** photo image (left) vs. vapor void fraction at mid-span section plane, by the modified SST model
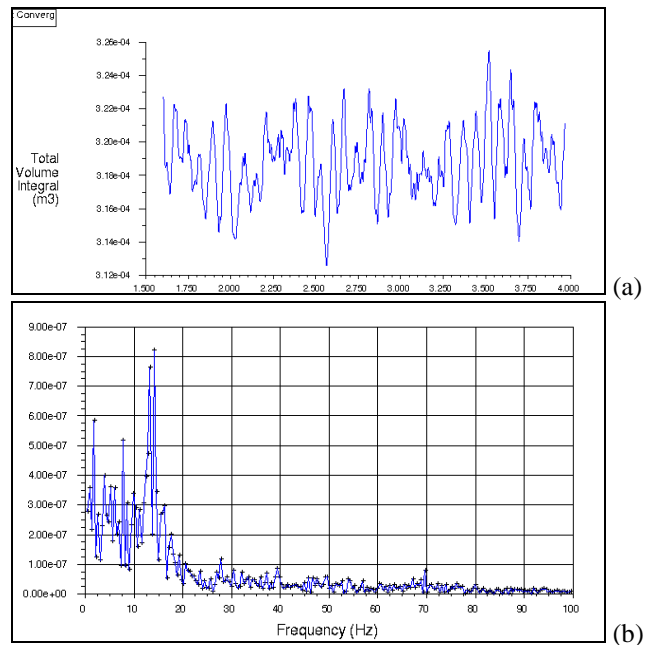

Figure 24: Time history of the total vapor volume (a); and spectral analysis of the vapor volume (b), by the modified SST model

11

By applying Reboud's modification to the existing SST k–ω model, a modified SST k–ω model is developed. For the 2D NACA0015 steady case (σ=1.6), the predicted cavity form and lift/drag are in reasonable agreement with the experiment. For the unsteady sheet cavitation (σ=1.0), the computation shows a multiple oscillating frequencies with the lowest dominant frequency being 3.5Hz, and the highest frequency (16.3Hz) being close to the measured value (~16Hz). Two shedding mechanism are recognized from the simulations: (a) Shedding of medium to large scale cavities due to an upstream moving re-entrant jet and its interference with the external flow; (b) Shedding of small cavitation vortices downstream an upstream moving sheet cavity. The shed cavitation vortices can be potentially erosive for propellers and hydrofoils under certain conditions. The existence of this type of cavities was reconfirmed in a recent experiment at SSPA [22].

For the 3D twisted foil, the modified SST model together with Singhal's cavitation model improves the RANS solver's possibility to predict the essential features like re-entrant jets and shedding of macro scale cloud structures observed in the experiment. Though calculations are performed on a coarse grid, the time-averaged lift coefficient is fairly close to the measured one. The predicted shedding frequency reveals multi-frequency character. Further study with a fine mesh is planned.

Reboud's modification, although being an artificial correction model, can bring down the eddy viscosity to a more reasonable level than the standard SST k-ω model would give, and therefore makes it possible to predict the shedding behavior of unsteady cavitation to a level at least qualitatively in agreement with experiment observations. Though the shedding frequency, the global lift and drag coefficients predicted by the modified model are still not accurate enough, they show a correct trend or response with variation of cavitation numbers. There is still a room for tuning the model constant (not studied here) for improvement. Before any new turbulence model that is dedicated to the multiphase cavitating flow is developed, the present approach has the potential for practical industrial applications. At least the approach is applicable for the RANS solver in FLUENT.

ACKNOWLEDGMENTS

NOMENCLATURE

C_L, C_D	Lift and drag coefficient
C_p	Pressure coefficient,
f	Shedding frequency
p	Static pressure at point of interest
p_0	Reference pressure at infinity
p_v	Vapour pressure
V_0	Free stream velocity
St	Strouhal number, $St = fc/V_0$
y^+	Non-dim. wall distance of 1st grid cell layer
α	Volume fraction
k	Turbulent kinetic energy
ω	Specific dissipation rate
μ_t	Turbulent viscosity
v_r	Turbulent viscosity ratio, $v_r = \mu_t/\mu$
d_r	Water-to-vapor density ratio, ρ_l/ρ_v
ρ	Density
σ	Cavitation number, $\sigma = 2(p_0 - p_v)/(\rho V_0^2)$

REFERENCES

[1] Bark, G., Grekula, M., Bensow, R. E. and Berchiche, N. 2009, "On Some Physics to Consider in Numerical Simulation of Erosive Cavitation", The 7th Int. Symp. on Cavitation (CAV2009), Ann Arbor, USA.

[2] Bark, G., Berchiche N., and Grekula M. 2004, "Application of principles for observation and analysis of eroding cavitation – EROCAV observation handbook", Ed. 3.1, Chalmers Univ. of Technology, Sweden.

[3] Foeth, E.-J. and Terwisga, T. van 2006, "The structure of unsteady cavitation. Part I: Observations of an attached cavity on a 3-dimensional hydrofoil", Sixth International Symposium on Cavitation, (CAV2006), The Netherlands.

[4] Senocak, I. and Shyy, W. 2004, "Interfacial dynamics-based modeling of turbulent cavitating flows, Part-2: time-dependent computations", Int. J. Numer. Meth. Fluids, Vol. 44, pp 997-1016.

[5] Venkateswaran, S., Lindau, J., Kunz, R. and Merkle C. 2002, "Computation of Multiphase Mixture Flows with Compressibility Effects", Journal of Computational Physics, Vol. 180, pp. 54-77.

[6] Reboud, J.L., Stutz, B. and Coutier, O., 1998, "Two-phase flow structure of cavitation: Experiment and modelling of unsteady effects", Proc. of the 3rd International Symposium on Cavitation, Grenoble, France.

[7] Coutier-Delgosha, O. Fortes-Patella, R. and Reboud, J.L. 2002, "Simulation of unsteady cavitation with a two-equation turbulence model including compressibility effects", Journal of Turbulence, 3 (2002) 058.

[8] Coutier-Delgosha, O., Reboud, J.L., and Fortes-Patella, R., 2003, "Evaluation of the Turbulence Model Influence on the Numerical Simulations of Unsteady Cavitation", Journal of Fluids Engineering, Vol. 125, pp. 38-45.

[9] Dular, M., Bachert, R., Stoffel, B. and Sirok, B., 2003, "Numerical and experimental study of cavitating flow on 2D and 3D hydrofoils", Fifth International Symposium on Cavitation (CAV2003), Osaka, Japan.

[10] Wu, J., Utturkar, Y., Senocak, I., Shyy, W. and Arakere, N. 2003, "Impact of turbulence and compressibility modeling on three-dimensional cavitating flow computations", AIAA 2003-4264.

[11] Wu, J., Wang, G., and Shyy, W. 2005, "Time-dependent turbulent cavitating flow computations with interfacial transport and filter-based models", Int. J. Numer. Meth. Fluids, Vol. 49, pp. 739-761.

[12] Ait Bouziad, Y., 2005, "Physical modeling of leading edge cavitation: computational methodologies and application to hydraulic machinery", Ph. D. thesis, EPFL, France.

[13] Li, D-Q and Grekula M., 2008, "Prediction of dynamic shedding of cloud cavitation on a 3D twisted foil and comparison with experiments", *The 27th Symposium of Naval Hydrodynamics*, Seoul, Korea.

[14] Menter, F.R., 1994, "Two-Equation Eddy-Viscosity Turbulence Models for Engineering Applications", *AIAA Journal*, 32(8):1598-1605.

[15] Huuva, T. 2008, "Large eddy simulation of cavitating and non-cavitating flow", PhD thesis ISBN/ISSN: 97891-73850636, Chalmers University of Technology, Sweden.

[16] Schnerr, G. H. and Sauer J., 2001, "Physical and Numerical Modeling of Unsteady Cavitation Dynamics", In *Fourth International Conference on Multiphase Flow*, New Orleans, USA.

[17] Singhal, A. et al, 2002, "Mathematical Basis and Validation of the Full Cavitation Model", *Journal of Fluids Engineering,* Vol. 124.

[18] Sorguven, E. and Schnerr G. H. 2003, "Modified $k - \omega$ Model for Simulation of Cavitating Flows", *Proc. Appl. Math. Mech. **2***, 386–387.

[19] Basuki W., Schnerr, G.H. and Yuan ,W. 2002, "Single-phase and Modified Turbulence Models for Simulation of Unsteady Cavitating Flows", *Proceedings of the German-Japanese Workshop on Multi-Phase Flow*, Karlsruhe, Germany.

[20] Kjeldsen, M., Arndt, R. E. A., and Effertz, M. 2000, "Spectral Characteristics of Sheet/Cloud Cavitation", *J. Fluid Eng.,* Vol. 122, pp. 481-487.

[21] Lu, N.X., Bensow, R.E., Bark, G. and Berchiche N. 2008 "Large Eddy Simulations of Cavitating Flow around a 2D NACA0015 Using OpenFOAM", The 2nd VIRTUE-WP4 workshop on CFD for cavitating flows.

[22] Grekula, M. and Bark, G, 2009, "Experimental study of development of erosive cavitation on the SSPA propeller P1477 and related 2D foil", *VIRTUE Deliverable D4.4.2a*, SSPA and Chalmers Univ. of Technology, Sweden.

[23] Hoekstra, M. and Vaz, G. 2009, "The partial cavity on a 2D foil revisited", The 7th *Int. Symp. on Cavitation* (CAV2009), Ann Arbor, USA.

[24] Vaz, G., Rijpkema, D., Hoekstra, M., 2009 "A Theoretical, Numerical and Validation Study on Cavitation Models using a Multi-Phase URANS Code" The 7th *Int. Symp. on Cavitation* (CAV2009), Ann Arbor, USA.

[25] Larsson, L., Stern, F. and Bertram V. 2000, "Gothenburg 2000: a workshop on numerical ship hydrodynamics", *Chalmers Univ. Techn.*, Sweden.

[26] Hino, T. (editor), 2005, "CFD Workshop Tokyo", *National Maritime Research Institute,* Tokyo, Japan.

[27] Schnerr, G.H., Schmitdt S., Sezal, I. and Thalhamer, M., 2006 "Shock and wave dynamics of compressible liquid flows with special emphasis on unsteady load on hydrofoils and on cavitation in injection nozzles", Invited Lecture, *Sixth International Symposium on Cavitation, CAV2006*, The Netherlands.